Title No. 113-S53

# Seismic Repair of Severely Damaged Precast Reinforced Concrete Bridge Columns Connected with Grouted Splice Sleeves

by Joel E. Parks, Dylan N. Brown, M. J. Ameli, and Chris P. Pantelides

*A repair technique for severely damaged precast reinforced concrete (RC) bridge columns with grouted splice sleeve (GSS) connections has been developed that uses a carbon fiber-reinforced polymer (CFRP) shell and epoxy-anchored headed bars to relocate the column plastic hinge. Four original specimens were built using an accelerated bridge construction (ABC) technique with two different GSS systems and were tested to failure using cyclic quasi-static loads. One GSS system was used to connect an RC bridge pier cap to a column and the second GSS system was used to connect an RC footing to a column. Failure of the four original specimens occurred at drift ratios between 5.6 and 8.0% with longitudinal bar fracture or pullout from the GSS connections. The repair method successfully relocated the plastic hinge to the original column section adjacent to the repair and was capable of restoring the diminished load and displacement capacity. The method is a viable and cost-effective technique for rapid seismic repair of severely damaged precast bridge assemblies.*

**Keywords:** accelerated bridge construction; bridge; earthquake; fiber-reinforced polymer composite; plastic hinge relocation; rehabilitation; repair; seismic; strengthening.

## INTRODUCTION

Repair of severely damaged bridge elements following an earthquake is an advantageous alternative to replacement; the benefits include cost savings, reduction in construction time, and decreased interruption for emergency services and the general public. The objective of bridge repair is to rehabilitate damaged bridge elements to a performance level similar to their original performance by restoring the load and displacement capacity of the system. Capacity-based bridge design directs damage to bridge columns, thus protecting the pier caps and footings; hence, the post-seismic repair studied is focused on column repair. Repair techniques for damaged bridge columns include the use of externally bonded carbon fiber-reinforced polymer (CFRP) jackets,[1-6] steel jackets,[7-9] and concrete jackets.[10,11] However, until recently it has been assumed that when longitudinal bars within the column buckle or fracture, the column should be replaced.[12]

Accelerated bridge construction (ABC) is gaining acceptance because of reduced construction time and minimal traffic interruption. Grouted splice sleeves (GSSs) have been gaining attention as a possible precast concrete connection method for ABC in seismic regions. Researchers are currently investigating the performance of GSS connections for bridges built in seismic regions.[13-15] The use of GSS connections in moderate to high seismic regions is imminent, and a practical post-earthquake repair is needed to accompany this new technology. Findings from the current ABC research indicate that columns connected using GSS connectors concentrate the column damage and decrease the effective plastic hinge length compared to traditional monolithic construction, especially if GSS connectors are incorporated in the column ends.[16] These damage characteristics are advantageous for repair purposes, leaving a relatively undamaged column section for plastic hinge relocation.

The repair method developed has been designed and implemented on four severely damaged precast specimens connected using GSS connectors. The specimens had undergone quasi-static cyclic loading, reaching a final damage state before being repaired. The repair uses materials that are available and easy to install, including epoxy-anchored headed bars, CFRP sheets, and nonshrink or expansive concrete.[17] The result is a cost-effective, corrosion-resistant, rapid repair method that could be installed within a few days. Due to the robust nature of the repair method, it is a suitable option for columns of varying damage states, including columns with buckled or fractured longitudinal bars.

## RESEARCH SIGNIFICANCE

There are very few studies for the repair of severely damaged concrete columns after earthquakes. The rehabilitation method described in this paper concerns connections between precast columns and footings, and precast columns and pier caps. This research uses high-performance materials, including headed reinforcing bar, epoxy, nonshrink or expansive concrete, and carbon fiber sheets to repair damaged columns constructed using ABC techniques. Although the repair was developed for precast concrete elements connected with grouted splice sleeves, it could be extended to seismically retrofit and repair existing columns as well. It has the potential to be used in the retrofit of column connections before an earthquake as well as a rapid repair method for such column connections after an earthquake.

## EXPERIMENTAL INVESTIGATION OF ORIGINAL SPECIMENS

### Original test specimens

Four precast RC specimens representing half-scale bridge elements, conforming to current seismic bridge design stan-

*ACI Structural Journal*, V. 113, No. 3, May-June 2016.
MS No. S-2015-173, doi: 10.14359/51688756, was received May 27, 2015, and reviewed under Institute publication policies.  Pertinent discussion including author's closure, if any, will be published ten months from this journal's date if the discussion is received within four months of the paper's print publication.

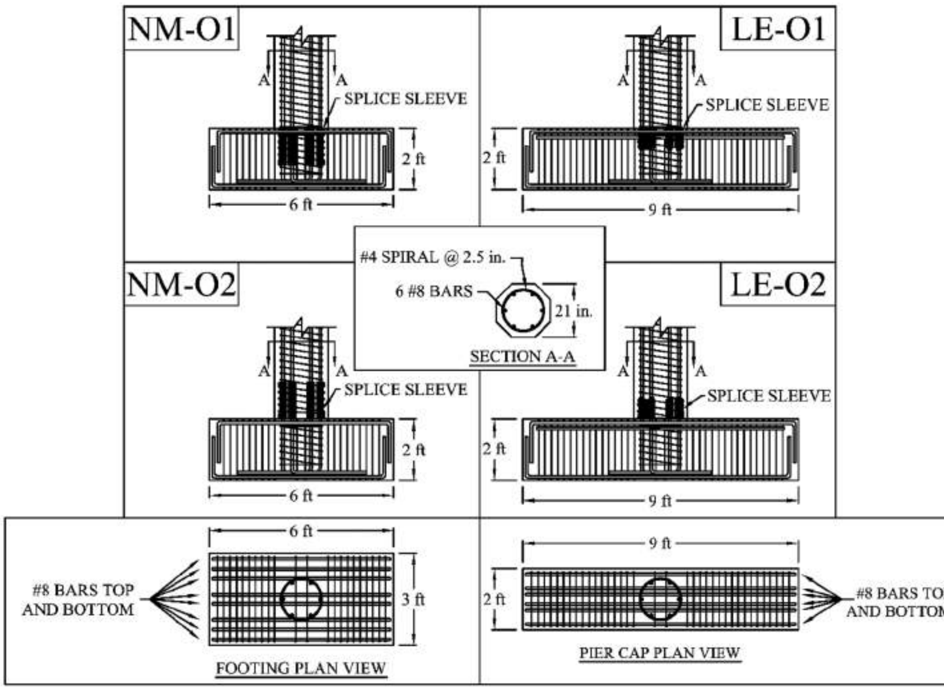


*Fig. 1—Original specimen reinforcement and geometry. (Note: 1 ft = 304 mm; 1 in. = 25.4 mm.)*

**Table 1—Material properties**

| Material properties | | NM-O1 | NM-R1 | NM-O2 | NM-R2 | LE-O1 | LE-R1 | LE-O2 | LE-R2 |
|---|---|---|---|---|---|---|---|---|---|
| Longitudinal bars | $f_y$, ksi (MPa) | 68 (469) | 68 (469) | 68 (469) | 68 (469) | 68 (469) | 68 (469) | 75 (517) | 75 (517) |
| | $f_u$, ksi (MPa) | 93 (641) | 93 (641) | 93 (641) | 93 (641) | 93 (641) | 93 (641) | 103 (710) | 103 (710) |
| Concrete compressive strength | Test day, ksi (MPa) | 5.5 (38) | 6.4 (44) | 8.4 (58) | 9.3 (41) | 6.0 (41) | 6.1 (42) | 8.2 (57) | 9.4 (65) |

dards,[18] were constructed using two different GSS systems. Specimens NM-O1 and NM-O2 are column-to-footing assemblies connected with a GSS system that uses high-strength, nonshrink grout on both ends of the sleeve to splice the bars from the footing and column. Specimens LE-O1 and LE-O2 are column-to-pier cap assemblies connected using a GSS system that uses a threaded connection on one end of the sleeve and a grouted connection on the other. The ID nomenclature for test specimens is as follows: the first two letters represent the splice sleeve type—GSS with both ends grouted is called NM, and GSS with one end threaded and one grouted is called LE; the letter "O" stands for original specimens.

The geometry and reinforcement of the original test specimens is shown in Fig. 1. The columns are 8.5 ft (2.59 m) tall with a 21 in. (533 mm) wide octagonal cross section. The longitudinal reinforcement consists of six No. 8 (25 mm) Grade 60 (414 MPa) bars arranged in a circular pattern. The GSS connectors are located in the footing and pier cap for NM-O1 and LE-O1, respectively, and in the columns for NM-O2 and LE-O2, respectively. A No. 4 (13 mm) Grade 60 (414 MPa) spiral at a 2.5 in. (64 mm) pitch is provided for transverse column reinforcement. The footing is 6 ft (1.82 m) long, 2 ft (610 mm) deep, and 3 ft (914 mm) wide. The pier cap is 9 ft (2.74 m) long, 2 ft (610 mm) deep, and 2 ft (610 mm) wide. The material properties for the precast RC components and the repair are given in Table 1.

## Testing assembly and loading protocol

In the test assembly, shown in Fig. 2, a lateral load is applied at a point that represents the inflection point of a bridge column. The footing and pier cap have spans of 4 and 8 ft (1.22 and 2.44 m), respectively. The pier cap specimen was tested upside down, with the pier cap on the strong floor, for ease of testing. The loading consisted of a constant axial load equal to 6% of the axial load capacity of the column and a displacement-controlled, cyclic, quasi-static lateral load. The lateral load was applied using the loading protocol shown in Fig. 3. Two cycles per drift ratio were used and the amplitude was progressively increased until a minimum 20% drop in the lateral load capacity was reached.[19]

## Original test specimen results

The damage state of the specimens prior to repair is a critical parameter for the repair design and subsequent performance. The initial test results of NM-O1, NM-O2, LE-O1, and LE-O2 are summarized in Table 2 in terms of maximum lateral load, ultimate drift ratio, displacement ductility, reserve capacity, and failure mode. The failure mode of NM-O1, NM-O2, and LE-O1 was fracture of an extreme longitudinal bar, whereas LE-O2 failed due to multiple longitudinal bars pulling out from the GSS connections in the column. The extreme east longitudinal bar fractured in both NM-O1 and NM-O2. The extreme west longitudinal bar fractured in LE-O1. At failure of all four original specimens, the lateral load capacity dropped well below 80% of

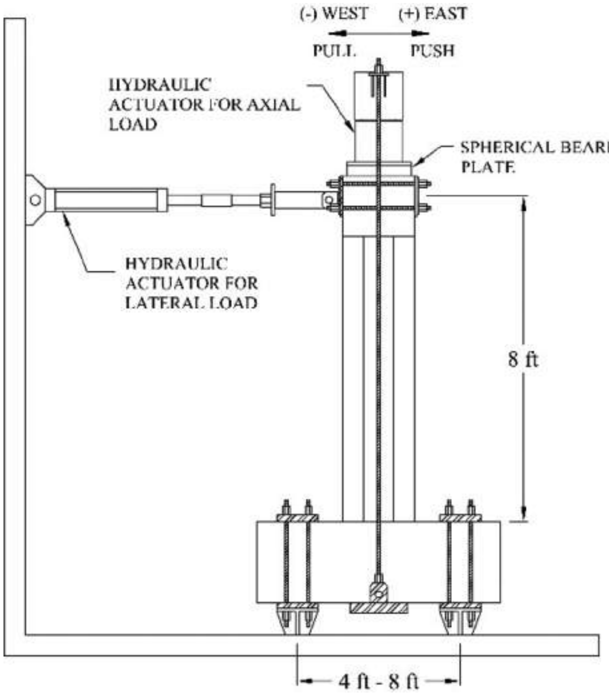


*Fig. 2—Test assembly. (Note: 1 ft = 304 mm.)*

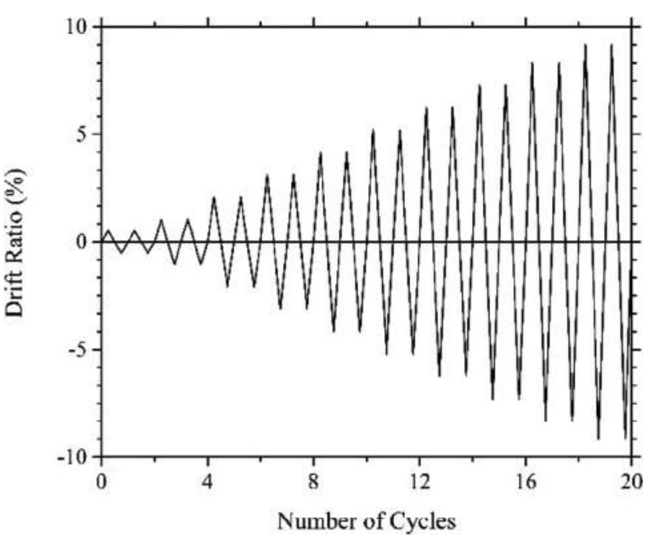


*Fig. 3—Loading protocol.*

the ultimate load. The reserve lateral load capacity of the original columns after testing ranged from 44 to 65% of the maximum lateral load capacity. Figure 4 shows the original column damage at the footing-to-column and column-to-pier cap interfaces, where extensive spalling and cracking occurred in the plastic hinge region. All original specimens experienced flexural cracking, which extended to 14 in. (356 mm) away from the footing or pier cap interface.

To assess the damage state of the original specimens a five-level performance evaluation approach was used.[20] This assessment procedure was based on the performance of the structure, which is defined by a particular damage state, and is classified into five levels. Level 1 is equivalent to no damage, and Level 5 is equivalent to local failure or collapse. According to this type of assessment, the four original specimens have reached a damage state designation of Level 5 because rein-

**Table 2—Original specimen test results**

| Test criteria | NM-O1 | NM-O2 | LE-O1 | LE-O2 |
|---|---|---|---|---|
| Maximum load, kip (kN) | 38.8 (173) | 42.0 (187) | 36.3 (161) | 44.8 (199) |
| Ultimate drift ratio, % | 6.69 | 7.91 | 6.50 | 6.00 |
| Displacement ductility | 6.1 | 6.8 | 5.8 | 3.1* |
| Reserve capacity, kip (kN) | 21.4 (95) | 23.6 (105) | 20.6 (92) | 15.9 (71) |
| Failure mode | East bar fracture | East bar fracture | West bar fracture | GSS bar pullout |

*Value is unnaturally low due to predamaged condition before testing.[15]

forcing bar fracture or pullout from the GSS occurred, thus significantly compromising the lateral load-carrying capacity of the columns. Structural components with a damage level of 5 usually require replacement. However, with the repair method developed, repair of precast columns connected using GSS connectors with Level 5 damage is possible.

## REPAIR DESIGN

The objective of the repair was to strengthen the original plastic hinge region and relocate the plastic hinge to a column section adjacent to the repair. This was done by increasing the 21 in. (533 mm) octagonal cross section to a reinforced 30 in. (762 mm) diameter circular cross section; the latter was constructed by post-installing epoxy-anchored headed bars for additional tensile force transfer and subsequently filling a carbon fiber-reinforced polymer (CFRP) shell with nonshrink or expansive concrete, as shown in Fig. 5. To form the new plastic hinge, a bending moment referred to as $M_{PH}$ must be reached at the desired plastic hinge location. In the present case, the original specimen test results were used to determine $M_{PH}$; however, it could be found using a sectional analysis as well. From Fig. 6, it can be seen that the bending moment demand experienced at the column joint, $M_{joint}$, is a function of the length of the repair, $H_{rep}$, and the distance from the point of inflection to the column-footing or column-pier cap joint, $H_{col}$. This relationship is shown in Eq. (1).

$$M_{joint} = \frac{M_{PH}}{\left(1 - \frac{H_{rep}}{H_{col}}\right)} \quad (1)$$

Similar to the bending moment demand, the shear force demand that must be resisted by the column to achieve plastic hinge relocation, $V_{PHR}$, is directly related to $H_{rep}$. This relationship is shown in Eq. (2).

$$V_{PHR} = \frac{M_{PH}}{(H_{col} - H_{rep})} \quad (2)$$

Equations (1) and (2) indicate that using the minimum possible repair height is advantageous for limiting the bending moment and shear demands. However, the height of the repair must be sufficient to relocate the new plastic hinge

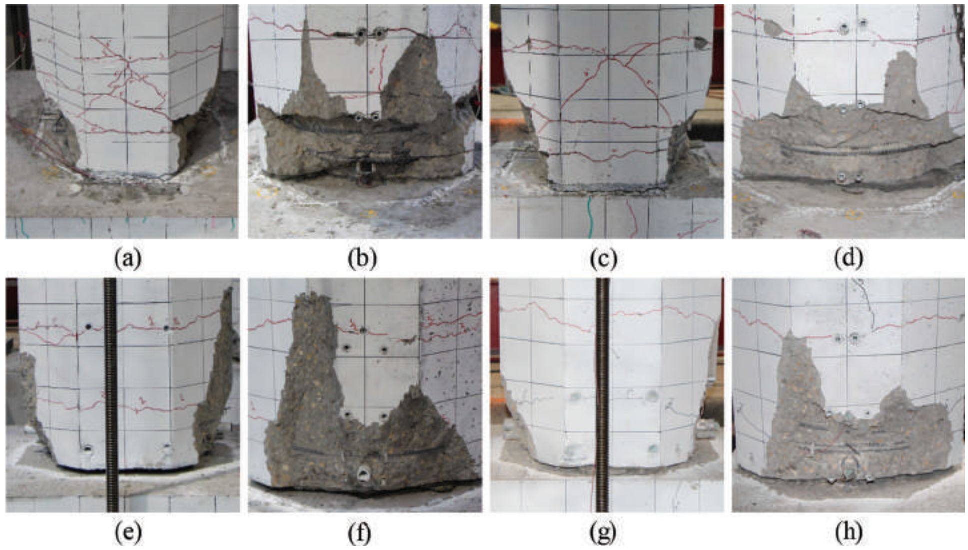


*Fig. 4–Original specimen damage: (a) NM-O1 (front); (b) NM-O1 (side); (c) LE-O1 (front); (d) LE-O1 (side); (e) NM-O2 (front); (f) NM-O2 (side); (g) LE-O2 (front); and (h) LE-O2 (side).*

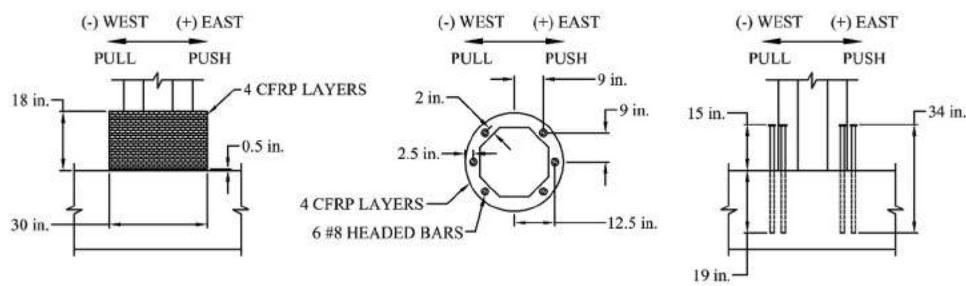


*Fig. 5—Repair design. (Note: 1 in. = 25.4 mm.)*

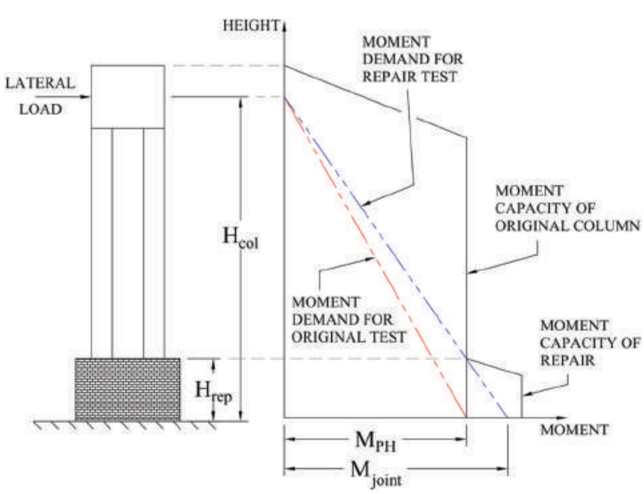


*Fig. 6—Moment demand.*

to a column cross section that has minimal damage. From the observed damage of the four original specimens shown in Fig. 4, a repair height of 18 in. (457 mm) was determined to be sufficient. In this case, there were two criteria to define the repair height. The first was to relocate the plastic hinge above any structural cracks equal to or larger than 0.01 in. (0.254 mm) wide, and the second was to provide enough height to develop the headed bars in tension.

Headed bars were designed to develop the increased joint moment, $M_{joint}$, required for the repair. The headed bar length drilled into the footing or pier cap was determined so that the epoxy anchorage would develop the yield stress of the bars in tension. Similarly, the length of headed bar extending into the repair satisfies adequate development length requirements according to AASHTO.[18] These parameters led to the design of six No. 8 (25 mm) Grade 60 (414 MPa) headed bars that were post-installed around the column, as shown in Fig. 5. The embedment into the footing or pier cap was 19 bar diameters and the length extending into the repair was 15 bar diameters. The headed bars used in this design had a head diameter of 2.25 in. (57 mm) and a yield strength of 62 ksi (427 MPa). A more detailed description of the headed bar design can be found in Brown[21] and Parks.[22]

The 30 in. (762 mm) diameter repair cross section used a CFRP shell that was designed to provide confinement, shear strength, and was also used as stay-in-place formwork for the nonshrink or expansive concrete. Four layers of unidirectional CFRP sheets oriented in the hoop direction were provided. One layer was provided to restore the shear strength of the original plastic hinge region, as given in Eq. (2); details of the design procedure are provided elsewhere.[21-23] Two layers were provided for adequate confinement and prevention of strain softening for the increased moment given in Eq. (1) and one layer was provided as a shell to wrap subsequent layers of CFRP around. A 0.5 in. (13 mm) gap was left between the bottom of the jacket and footing or pier cap surface, as shown in Fig. 5, to ensure there was no bearing of the CFRP shell on the concrete during large displacements. The ultimate tensile capacity of

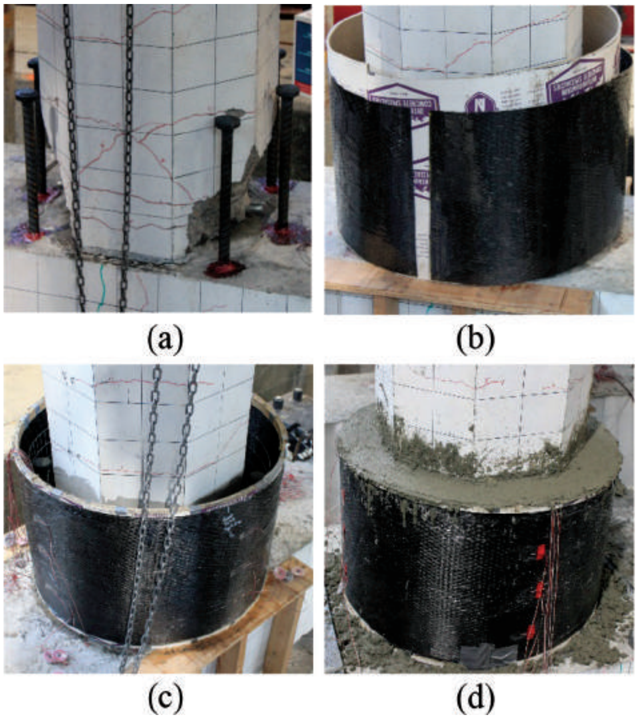


*Fig. 7—Repair procedure: (a) post-installed headed bars; (b) split CFRP shell; (c) CFRP shell around column; and (d) CFRP shell filled with nonshrink or expansive concrete.*

the CFRP composite was 101 ksi (696 MPa), the modulus of elasticity was 8990 ksi (62,000 MPa), and the ultimate strain was 1.12%, as determined by tensile coupon tests according to ASTM D3039.[24]

The shear capacity of the original column should be checked to ensure flexural failure at the location of the relocated plastic hinge. In the present investigation, the transverse reinforcement in the relocated plastic hinge was sufficient to produce a flexural failure mode. If however, the shear capacity of the column was insufficient, additional retrofit of the column in the relocated plastic hinge, and potentially the entire column length, would have been necessary. To aid in the design of the repair, a strut-and-tie model has been developed and is presented elsewhere.[21,22]

## Repair procedure

The first step in the repair procedure was to create a prefabricated CFRP shell. A single layer of 18 in. (457 mm) wide CFRP sheet impregnated with epoxy was wrapped and cured around a 30 in. (762 mm) diameter sonotube to create the proper shape. While the CFRP shell was curing, the holes for the headed bars were core drilled into the footing or pier cap and the headed bars were epoxy anchored into place around the column, as shown in Fig. 7(a). After the CFRP shell had cured, it was split into two half-cylinders and brought around the column, as shown in Fig. 7(b). The splitting and splicing of the first CFRP shell layer was performed to better simulate how the repair would be constructed in the field. A circular shell cannot be lowered over a column because the latter is connected to a footing and pier cap. The sonotube inside the shell in Fig. 7(b) was used to ensure that the shell maintained its shape, while the additional layers of CFRP were applied

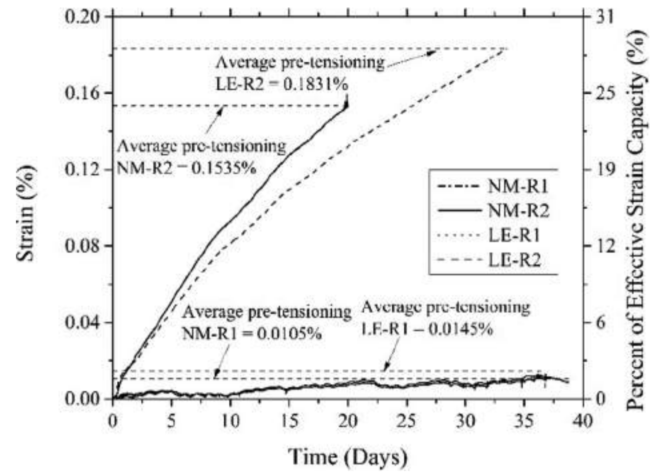


*Fig. 8—CFRP pretensioning.*

and subsequently removed once all CFRP layers had cured. A 12 in. (305 mm) long by 18 in. (457 mm) wide piece of CFRP sheet impregnated with epoxy was used to splice the two halves of the CFRP shell on both sides. Once the first layer of the CFRP shell was spliced, three additional CFRP layers were added, as shown in Fig. 7(c). Each layer was 100 in. (2.54 m) long by 18 in. (457 mm) wide, with a 6 in. (152 mm) overlap for each layer. This was the last step in completing the construction of the CFRP shell which acted as stay-in-place formwork for the repair concrete. Once the CFRP shell had fully cured, nonshrink or expansive concrete was added to the space between the column and CFRP shell, as shown in Fig. 7(d).

For LE-O1 and LE-O2, the diameter of the repair was larger than the width of the pier cap. Wooden forms were placed alongside the pier cap to provide sufficient width for the repair, as shown in Fig. 7(b) and 7(c). The wooden forms were removed once the concrete had cured. In practice, the pier cap would be oriented above the column, and the gap between the repair and pier cap would provide an inlet for the concrete; the gap between the column and the repair would have to be sealed.

## EXPERIMENTAL RESULTS OF REPAIRED SPECIMENS

Because the damage states of all original specimens prior to repair were similar, the repair design was used for all specimens. The repair method was implemented for NM-O1, NM-O2, LE-O1, and LE-O2, and the repaired specimens are referred to as NM-R1, NM-R2, LE-R1, and LE-R2, respectively; the "R" stands for "repaired" in the specimen ID. The only difference in the repair was the type of concrete used to fill the void between the original 21 in. (533 mm) octagonal column and the 30 in. (762 mm) diameter CFRP shell. This concrete, referred to as the repair concrete, was designed as nonshrink concrete for NM-R1 and LE-R1, and as expansive concrete for NM-R2 and LE-R2. The use of expansive, instead of nonshrink, concrete converts the CFRP shell from providing passive to active confinement. The difference in expansion among the repaired specimens can be seen by the amount of pre-tensioning experienced by the CFRP wrap prior to testing. Strain gauges were used to

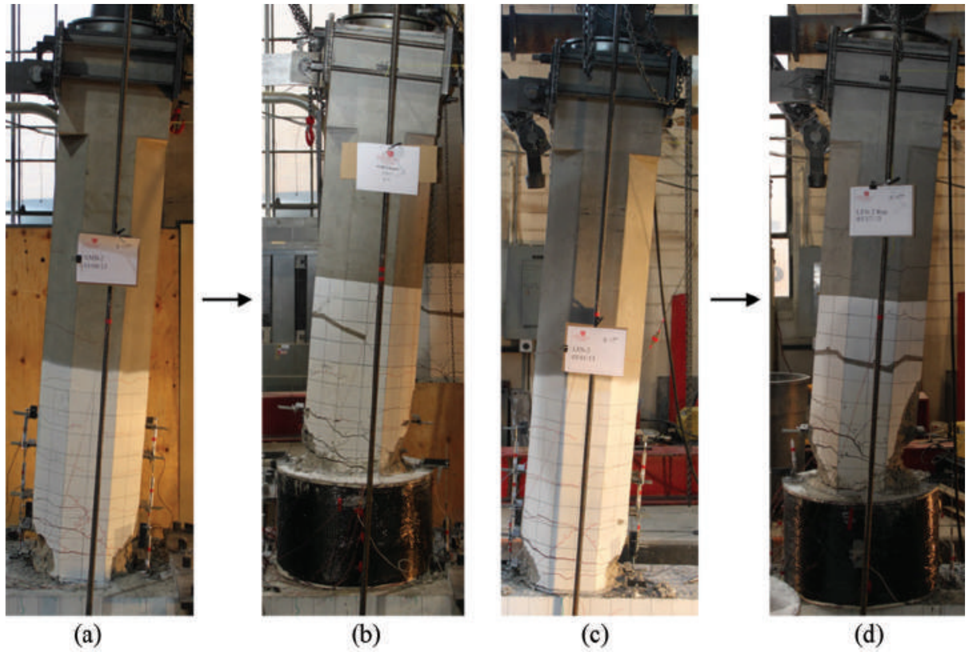


*Fig. 9—Plastic hinge relocation: (a) NM-01; (b) NM-R1; (c) LE-01; and (d) LE-R1.*

monitor this pre-tensioning for all repaired specimens up to 1 day prior to testing. The magnitude of pre-tensioning is shown in Fig. 8. Specimens NM-R1 and LE-R1, designed with nonshrink concrete, had low pre-tensioning between 0.015 and 0.016%, whereas Specimens NM-R2 and LE-R2, designed with expansive concrete, had significant pretensioning between 0.15 and 0.18%.

The test assembly and loading protocol remained unchanged for the original and repaired specimens. The strength and displacement capacity of the damaged bridge columns was restored by achieving the same displacement drift and lateral load as the original specimens. The successful plastic hinge relocation for NM-R1 and LE-R1 is shown in Fig. 9.

## Specimen NM-R1

The hysteretic response of NM-R1 superimposed with the hysteretic response of NM-O1 is shown in Fig. 10(a). It can be seen from the hysteretic response and Table 3 that NM-R1 achieved an 18% larger lateral load than NM-O1 and had a similar displacement capacity. The failure mode of NM-R1 was fracture of column longitudinal bars in the relocated plastic hinge region. The extreme west longitudinal bar fractured during the first cycle of the 7.3% drift step, and the extreme east longitudinal bar fractured during the second cycle of the same drift step. The east longitudinal bar fractured only 21.5 in. (546 mm) above the original fracture location in NM-O1; this implies that the repair provided sufficient confinement and clamping force to develop the longitudinal bar in a shorter distance than expected. Other major events included the onset of significant spalling at a 3.1% drift ratio and CFRP cracking parallel to the fiber direction at a drift ratio of 4.2%. The circumferential CFRP crack was located approximately 3 in. (76 mm) below the top of the shell, at the same level as the top of the headed bars, and extended halfway around the jacket circumference on the east side. This is the same side the longitudinal column

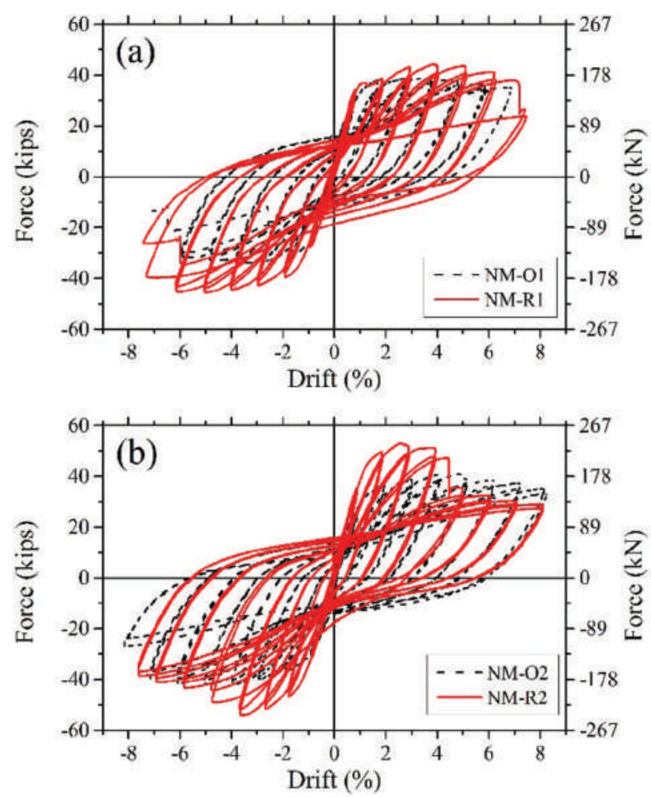


*Fig. 10—NM hysteretic response: (a) NM-R1 and NM-O1; and (b) NM-R2 and NM-O2.*

bar fractured in NM-O1. Figure 11 shows the circumferential CFRP crack traced with a white marker. The hysteretic response of the specimen was unaffected by the circumferential crack in the CFRP shell.

## Specimen NM-R2

The hysteretic response of NM-R2 superimposed with the hysteretic response of NM-O2 is shown in Fig. 10(b).

**Table 3—Repaired specimen test results**

| Test criteria | NM-R1 | NM-R2 (West) | NM-R2 (East) | LE-R1 (Monotonic) | LE-R1 (Cyclic) | LE-R2 |
|---|---|---|---|---|---|---|
| Maximum load, kip (kN) | 45.6 (203) | 54.2 (241) | 53.0 (236) | 46.8 (208) | 40.5 (180) | 50.5 (225) |
| Ultimate drift ratio, % | 6.96 | 5.89 | 4.60 | 6.88 | 7.20 | 6.17 |
| Displacement ductility | 6.0 | 3.9 | 3.9 | 6.6 | — | 4.6 |
| Failure mode | West and east bar fracture | West bar fracture | | — | East bar fracture | CFRP wrap fracture |

*Fig. 11—Circumferential CFRP crack (NM-R1).*

The failure mode of NM-R2 was fracture of the extreme west longitudinal bar during the 5.2% drift step. The lateral load capacity of NM-R2 was 28% higher than the lateral load capacity of NM-O2, as shown in Table 3. However, the displacement capacity of NM-R2 was less than that of NM-O2, at the ultimate displacement defined by a 20% drop in lateral load. The longitudinal column bar fracture, which caused the 20% drop in lateral load, was due to embrittlement from welding instrumentation fixtures to the bar. The brittle fracture of the bar was obvious through several characteristics. First, the fracture location was 10.5 in. (267 mm) above the top of the repair, which is significantly higher than the fracture location of all other tests, which occurred within 5 in. (127 mm) of the column-repair interface. Second, the fracture plane of the bar was smooth and level, which is a characteristic of a brittle steel fracture plane. Additionally, there was no decrease in diameter of the fractured bar when compared to the original bar diameter, indicating no necking had occurred prior to the fracture.

Although a 20% drop in lateral load-carrying capacity was observed, the test was carried out through the 8.3% drift step. From the hysteretic response, it can be seen that despite the mishap, NM-R2 performed quite well after the column bar had fractured, outperforming NM-O2 in the west direction of testing.

### Specimen LE-R1

In the case of Specimen LE-R1, a monotonic pushover was performed along with the loading protocol of Fig. 3. The monotonic load was applied to the column in the east direction until a drift ratio of 6.9% was reached. At this point, the column was brought back to its original vertical position and tested according to the loading protocol of Fig. 3. This series of loading emulates a near-fault ground motion that is characterized by an acceleration pulse followed by a sinusoidal-type ground motion.

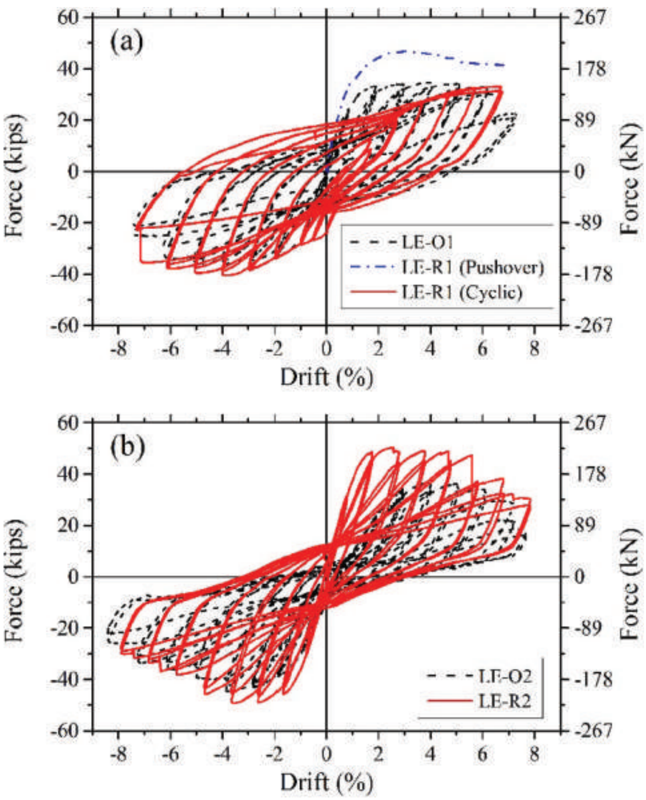


*Fig. 12—LE hysteretic response: (a) LE-R1 and LE-O1; and (b) LE-R2 and LE-O2.*

The monotonic pushover curve is shown in Fig. 12(a). Although the column was displaced to a drift ratio beyond the ultimate drift ratio of LE-O1, no longitudinal bars fractured in the column due to the monotonic nature of loading. There was major spalling on the east side of the column, as shown in Fig. 9(d), that extended 20 in. (508 mm) up the column and exposed the spiral reinforcement.

With the repaired column already damaged in one direction from the monotonic pushover test, the specimen was subsequently tested cyclically. The hysteretic response of LE-R1 is shown in Fig. 12(a) with the hysteretic response of LE-O1 superimposed. The right side of the hysteresis for LE-R1 shows an irregular response due to damage from the monotonic pushover. The left side of the hysteresis is minimally affected; comparisons of hysteretic response are made to this side of the hysteresis. The failure mode of LE-R1 was fracture of the extreme east longitudinal bar in the relocated plastic hinge region. The bar fractured during the first cycle of the 7.3% drift step. Similar to the behavior of NM-R1, the onset of significant spalling on the west side of the column occurred at a drift ratio of 3.1% and the onset of transverse CFRP cracking occurred at a drift ratio of 4.2%. The transverse CFRP cracking was located approximately 3 in. (76 mm) below the top of the shell, at the top of the headed bars, and extended halfway around the jacket circumference on the west side, similar to the crack shown in Fig. 11; this crack occurred on the same side as the longitudinal bar fracture in LE-O1. The specimen remained seemingly unaffected by the transverse CFRP crack.

Due to the initial damage of LE-R1 from the monotonic pushover, it is difficult to directly compare LE-R1 to LE-O1. However, by examining the performance of LE-R1 in Table 3 from both the monotonic pushover and cyclic tests, it is clear that LE-R1 performed similarly to LE-O1.

### Specimen LE-R2

The hysteretic response of LE-R2 superimposed with the hysteretic response of LE-O2 is shown in Fig. 12(b). During the 3.1% drift step, a transverse crack, which correlated with the top of the headed bars, occurred and extended over the entire circumference of the CFRP shell. Failure of LE-O2 was due to pullout of the longitudinal column bars on both column sides; this caused additional demand on the repair, causing a transverse crack on both sides.

Before the plastic hinge was completely relocated above the repair, the CFRP shell fractured. Fracture of the CFRP shell occurred during the first cycle of the 6.3% drift step, which caused a 20% drop in the lateral load. This fracture occurred directly below the top of the headed bars and the transverse CFRP crack on the northeast side of the repair. Although a 20% drop in lateral load-carrying capacity was observed during the 6.3% drift step, the test was continued through the 8.3% drift step. As the test progressed, the jacket fractured three additional times, with each fracture moving closer to the column pier cap interface.

Although the failure mode of LE-R2 was not the intended one and the plastic hinge was not relocated entirely above the repaired region, the specimen still showed a good hysteretic performance. The lateral load capacity of LE-R2 was 13% higher than the lateral load capacity of LE-O2. However, once the CFRP jacket had fractured, the hysteretic response of LE-R2 followed closely the response of LE-O2.

The reasons for failure of LE-R2 in the CFRP shell rather than in the column cross section adjacent to the repair are: 1) the GSS connectors are located in the column, leading to a different failure mode, which is pullout failure of the GSS system rather than reinforcing bar fracture. As such, the plastic hinge in LE-O2 is shorter than when the sleeves were located in the pier cap, as in LE-O1. With a shorter plastic hinge, damage does not spread up the column, implying that the repair could have been shorter, thus reducing the flexural demand in the repaired region; and 2) the strength of the column cross section adjacent to the repair; comparing material properties between LE-O1 and LE-O2, there was a 10% increase in the yield strength of the longitudinal bars and a 54% increase in the concrete compressive strength. The stronger column cross section combined with minimal damage of the original column increased the required moment capacity of the repair to higher levels than expected, thus causing failure to occur in the repair. Both reasons relate to the original damage state of the column. Therefore, the importance of having a good assessment of the damaged column strength cannot be overstated.

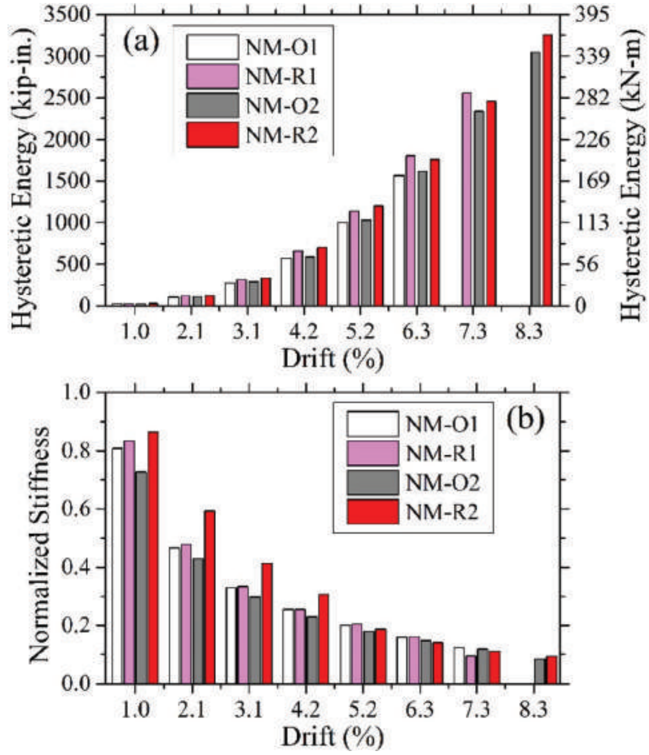


*Fig. 13—System performance: (a) cumulative energy dissipation; and (b) normalized stiffness degradation.*

## PERFORMANCE OF REPAIRED SPECIMENS

To further examine the performance of the repaired and original specimens, the cumulative hysteretic energy dissipation and stiffness degradation characteristics of the NM specimens are compared in Fig. 13. Specimens LE-O1 and LE-R1 are omitted due to the monotonic test of LE-R1, which affects the cyclic performance, thus causing an inaccurate comparison. Specimens LE-O2 and LE-R2 are also omitted due to the predamaged nature of LE-O2, thus causing an inaccurate comparison.[16] The cumulative energy dissipation of NM-R1 and NM-R2 is greater than that of their original counterparts for all drift ratios. At the completion of the 6.3% drift ratio, NM-R1 and NM-R2 dissipated 15% and 9% more energy than NM-O1 and NM-O2, respectively. Similarly, the stiffness degradation characteristics of NM-R1 and NM-R2 match the characteristics of NM-O1 and NM-O2, when normalized to the 0.5% drift step stiffness. This normalization was carried out to portray the degradation of stiffness rather than the numerical stiffness values because the repaired specimens have a higher stiffness due to the shorter column length and higher column concrete compressive strength. Both cumulative energy dissipation and stiffness degradation characteristics of the repaired specimens further confirm that the repair can restore the assembly to a performance level similar to the original condition.

Table 3 shows the test results for all repaired specimens. When these results are compared to Table 2 for the original

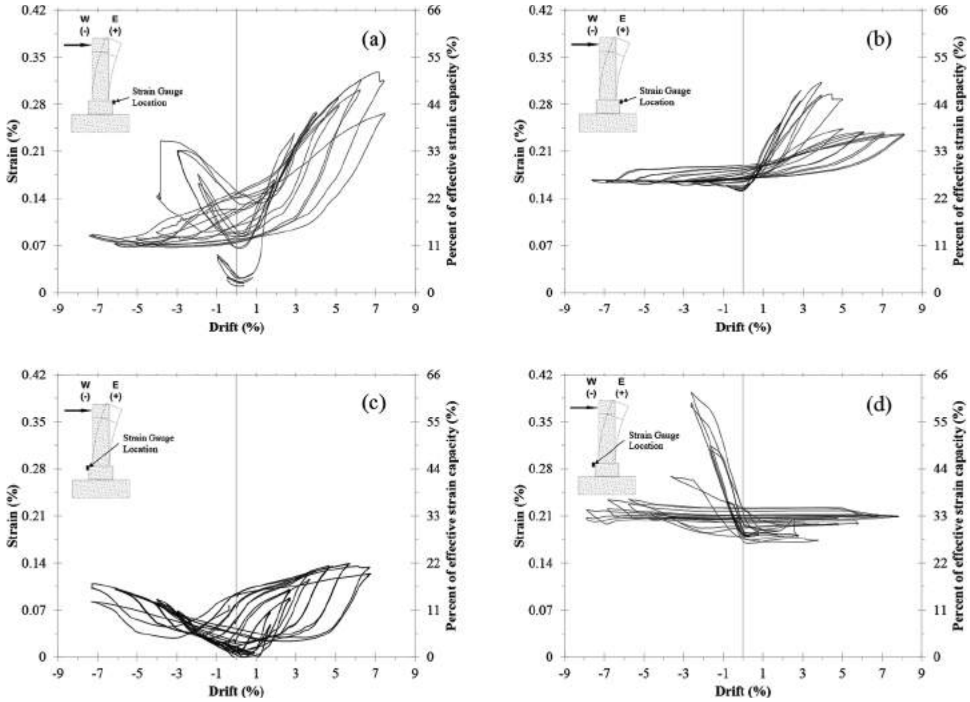


*Fig. 14—CFRP wrap strain 3 in. (76 mm) below top of repair: (a) NM-R1-East; (b) NM-R2-East; (c) LE-R1-West; and (d) LE-R2-West.*

columns, it can be observed that the repaired specimens were able to regain the strength achieved by the original specimens while still performing in a ductile manner in all cases.

## CFRP shell performance

The CFRP shell is a crucial component of the repair because it provides shear strength, peripheral tension, and confinement to the repaired section. The hoop strains from the tests are compared to the effective strain capacity of the CFRP jacket, as shown in Fig. 14. The strain efficiency factor for all repairs was taken as 57% of the ultimate strain capacity recorded from tensile coupon tests[25] and was used to determine the effective strain capacity. The CFRP strain efficiency factor accounts for strain concentrations, and the multiaxial state of stress acting on the jacket when the CFRP wrapped member is subjected to compression and bending.

*Nonshrink concrete*—The CFRP shell performance of NM-R1 and LE-R1 designed with nonshrink concrete is described first. Figure 14(a) shows that the hoop strain in the CFRP shell, 3 in. (76 mm) below the top of the repair for Specimen NM-R1, gradually increases until the 2.1% drift cycle. At this cycle, strains increase significantly, indicating that the CFRP shell is engaged. Radial cracks in the repair concrete originating from six of the eight column corners were observed on the surface of the repaired section at the end of the 1.0% drift cycle, as shown in Fig. 15. Due to the passive confinement present in the repair of NM-R1 and LE-R1, the radial cracks are necessary for the concrete to dilate and engage the CFRP shell; similar to NM-R1, radial cracks also appeared in LE-R1. LE-R1 displayed a different CFRP shell behavior, shown in Fig. 14(c), due to the fact that LE-R1 was loaded monotonically before the cyclic test. The radial cracks in the repair concrete were observed after the monotonic pushover, therefore, the repair concrete had already dilated and engaged the CFRP shell for the cyclic portion of the experiment. Due to the preexisting condition of the specimen before the cyclic test, residual hoop strains from the initial monotonic pushover were present similar to the residual hoop strains in NM-R1 after the 2.1% drift cycle.

*Fig. 15—Radial cracks in repair concrete (NM-R1).*

CFRP cracking parallel to the fiber direction occurred during the 4.2% drift step for both the NM-R1 and LE-R1 specimens. The circumferential CFRP crack was located approximately 3 in. (76 mm) below the top of the CFRP shell, which correlates to the top of the headed bars, and extended halfway around the jacket circumference. The circumferential CFRP crack also occurred on the side where the column longitudinal bar had fractured in NM-O1 and LE-O1. While the hysteretic response of both specimens remained unaffected from the circumferential crack in the CFRP, it did affect the performance of the CFRP shell. In Fig. 14(a), the CFRP shell engages in both directions until a sudden drop in

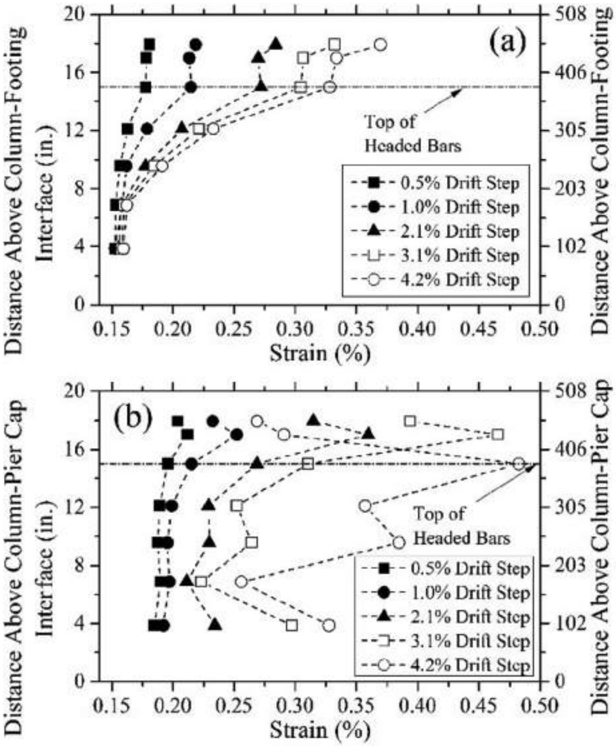


*Fig. 16—Wrap strain profile on west face: (a) NM-R2; and (b) LE-R2.*

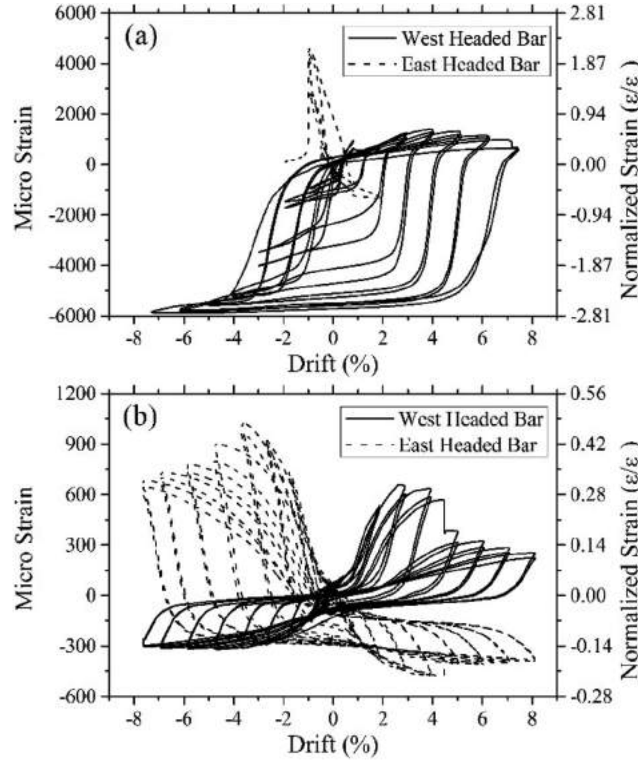


*Fig. 17—Headed bar strain: (a) NM-R1; and (b) NM-R2.*

strain is observed at a drift of 4.2%, correlating to the onset of the circumferential crack. The crack occurred due to a lack of tension capacity in the repair concrete above the headed bars; this cracking could be mitigated by using bidirectional CFRP or fiber-reinforced concrete, which provides additional tension capacity perpendicular to the CFRP fiber direction.

*Expansive concrete*—A much different CFRP shell performance was observed when expansive concrete was used to achieve active confinement for Specimens NM-R2 and LE-R2. In Fig. 14(b) and 14(d) the CFRP shell is engaged from the start of the test; there were no observed radial cracks in the repaired concrete for both specimens. The expansive concrete generated sufficient dilation in the CFRP shell before any lateral load was applied, as shown in Fig. 8, thus eliminating the need for damage to occur before the CFRP engaged. However, control of concrete expansion is critical, as excessive initial expansion reduces the remaining strain capacity of the CFRP shell.

For Specimens NM-R2 and LE-R2 a series of strain gauges orientated in the hoop direction were placed on the west side of the CFRP shell at different elevations. The strain profile in Fig. 16(a) is a plot of strain gauge height above the footing for Specimen NM-R2 versus maximum hoop strain during a drift step; the points at a given drift step are connected with a dashed line. The strain in the CFRP shell of NM-R2 increases significantly up to a height of 15 in. (381 mm) above the top of the footing. The discontinuity observed at 15 in. (381 mm) is due to termination of the headed bars at that elevation. This demonstrates the contribution of the headed bars in the overall stress transfer mechanism.[21,22]

The strain profile for LE-R2 in Fig. 16(b) is similar to that of NM-R2 in the first two drift steps. At the 2.1% drift step, large strains began to occur 17 in. (432 mm) away from the pier cap interface and continued to increase during the 3.1% drift step. At the end of the 3.1% drift cycle, a transverse crack developed that propagated for the entire circumference of the CFRP shell. The strain profile at the 4.2% drift step indicates that once the circumferential crack had fully developed, the strain demand had transferred from 17 to 15 in. (432 to 381 mm) above the pier cap. Because the strain was concentrated at the top of the headed bars, the tensile capacity of the jacket was exceeded at this level, causing the first fracture of the CFRP jacket.

## Headed bar performance

The post-installed headed bars are a critical component of the force transfer mechanism required to relocate the plastic hinge. The headed bars provide a means to transfer tension from the column to the footing or pier cap; this was lost when the column longitudinal bars fractured in the original specimens. A strain gauge was placed on the extreme east and west headed bars 7.5 in. (191 mm) from the top of the footing for Specimens NM-R1 and NM-R2 to monitor the strain. Figure 17 shows the results from these gauges for NM-R1 and NM-R2. Figure 17(a) shows that the east headed bar yielded in tension during the 1.0% drift step reaching strains above 1.9 times the yield strain. After the 1.0% drift step, the east strain gauge was lost; however, it is clear that the east headed bar went well beyond 1.9 times the yield strain in subsequent drift steps. The west headed bar yielded in compression during the 3.1% drift step, reaching compressive strains 2.8 times the yield strain during the 7.3% drift step.

In Fig. 17(b), a much different headed bar occurred; the maximum tensile strain recorded during the test of NM-R2 was 0.44 times the yield strain. This is unlike NM-R1, where tensile strains on the headed bars reached well beyond yield. The difference in headed bar response is attributed largely to the concrete type used in the repair. The use of expansive concrete to create an active confinement system was able to not only increase the compressive strength of the concrete, but also its tensile strength. With the expansive concrete having a higher tensile capacity, the demand on the headed bars of NM-R2 was reduced significantly compared to the headed bars of NM-R1 with nonshrink concrete.

## CONCLUSIONS

A method has been developed for post-earthquake repair of severely damaged bridge columns connected using GSS connectors located in the column, footing, and pier cap. The severe damage includes fractured column bars and extensive concrete spalling. The repair converts the original plastic hinge region of the 21 in. (533 mm) octagonal column to a 30 in. (762 mm) diameter circular cross section, thereby relocating the new plastic hinge to a minimally damaged section adjacent to the repair. This repair procedure was implemented and tested on cyclically damaged precast bridge column-to-footing and column-to-pier cap assemblies; it was capable of restoring the diminished performance of the specimens in terms of lateral displacement, lateral load, energy dissipation, and stiffness.

The important components of the repair were the CFRP shell, the post-installed headed steel bars, and the repair concrete inside the shell. The CFRP shell provided confinement, shear strength, and peripheral tension to the repair, especially at the top of the CFRP shell. The post-installed headed bars were successful in providing sufficient flexural capacity in the repaired region to relocate the plastic hinge. The headed bars also provided a means to transfer the tension lost by the fractured original column longitudinal bars connecting the columns to the footing or pier cap. Both nonshrink and expansive concrete were successful in restoring the capacity of the column.

The nonshrink concrete with the CFRP shell provided sufficient passive confinement. The expansive concrete with CFRP shell provided active confinement. The use of expansive instead of nonshrink concrete caused sufficient dilation to produce an active confinement system. The additional confining pressure gained with active confinement increased tensile capacity, which helped negate circumferential CFRP shell cracking and the tensile demand on the headed bars. However, control of the amount of concrete expansion is important, as excessive initial expansion will reduce the remaining tensile capacity in the CFRP shell.

Based on the overall performance of the repair in the half-scale experiments, this is a viable repair technique for damaged columns in moderate to high seismic regions. In the present case, initial damage of the columns was severe; therefore, the method is deemed to be robust and is applicable to columns with varying damage states. The repair technique is rapid and thus satisfies the requirements of accelerated bridge construction.

## AUTHOR BIOS

**Joel E. Parks** *is a PhD Candidate in the Department of Civil and Environmental Engineering at the University of Utah, Salt Lake City, UT. He received his bachelor's degree from Boise State University, Boise, ID, and his MS degrees from the University of Utah. His research interests include repair of reinforced concrete structures and evaluation of structures anchored to concrete.*

**Dylan N. Brown** *is a Bridge Engineer at Michael Baker International, Madison, WI. He received his bachelor's degree and MS in structural engineering from the Civil and Environmental Engineering Department at the University of Utah. His research interests include nonlinear design and analysis of reinforced concrete structures, and application of composites in repair and retrofit.*

*ACI member* **M. J. Ameli** *is a PhD Candidate at the Civil and Environmental Engineering Department of the University of Utah, where he also received his MS. He received his BS from Sharif University of Technology, Tehran, Iran. His research interests include experimental evaluation and analytical modeling of reinforced/precast concrete components, seismic design and analysis of reinforced/precast concrete structures, and application of composites in repair and retrofit of concrete components.*

*ACI member* **Chris P. Pantelides** *is a Professor in the Civil and Environmental Engineering Department of the University of Utah. His research interests include seismic design and rehabilitation of reinforced concrete, precast and prestressed concrete buildings and bridges, and the application of fiber-reinforced polymer composites.*

## ACKNOWLEDGMENTS

The authors would like to thank the Utah Department of Transportation, New York State Department of Transportation, Texas Department of Transportation, and the Mountain Plains Consortium for their financial support. The authors would also like to thank NMB Splice Sleeve, Erico, Sika, and Headed Reinforcement Corp. for their donation of construction materials.

## NOTATION

$H_{col}$ = distance from point of inflection to column-footing or column-pier cap joint
$H_{rep}$ = length of repair
$M_{joint}$ = bending moment to cause plastic hinge at original column joint
$M_{PH}$ = bending moment to cause plastic hinge at new plastic hinge location
$V_{PHR}$ = column shear force to plastic hinge relocation

## REFERENCES

1. Seible, F.; Priestley, M.; Hegemier, G.; and Innamorato, D., "Seismic Retrofit of RC Columns with Continuous Carbon Fiber Jackets," *Journal of Composites for Construction*, ASCE, V. 1, No. 2, 1997, pp. 52-62. doi: 10.1061/(ASCE)1090-0268(1997)1:2(52)

2. Saadatmanesh, H., Ehsani. M.; and Jin, L., "Repair of Earthquake-Damaged RC Columns with FRP Wraps," *ACI Structural Journal*, V. 94, No. 2, Mar.-Apr. 1997, pp. 206-215.

3. Gergely, I.; Pantelides, C.; Nuismer, R.; and Reaveley, L., "Bridge Pier Retrofit Using Fiber-Reinforced Plastic Composites," *Journal of Composites for Construction*, ASCE, V. 2, No. 4, 1998, pp. 165-174. doi: 10.1061/(ASCE)1090-0268(1998)2:4(165)

4. Xiao, Y.; Wu, H.; and Martin, G. R., "Prefabricated Composite Jacketing of RC Columns for Enhanced Shear Strength," *Journal of Structural Engineering*, ASCE, V. 125, No. 3, 1999, pp. 255-264. doi: 10.1061/(ASCE)0733-9445(1999)125:3(255)

5. Pantelides, C.; Gergely, J.; Reaveley, L.; and Volnyy, V., "Retrofit of RC Bridge Pier with CFRP Advanced Composites," *Journal of Structural Engineering*, ASCE, V. 125, No. 10, 1999, pp. 1094-1099. doi: 10.1061/(ASCE)0733-9445(1999)125:10(1094)

6. Pantelides, C.; Alameddine, F.; Sardo, T.; and Imbsen, R., "Seismic Retrofit of State Street Bridge on Interstate 80," *Journal of Bridge Engineering*, ASCE, V. 9, No. 4, 2004, pp. 333-342. doi: 10.1061/(ASCE)1084-0702(2004)9:4(333)

7. Chai, Y.; Priestley, N.; and Seible, F., "Seismic Retrofit of Circular Bridge Columns for Enhanced Flexural Performance," *ACI Structural Journal*, V. 88, No. 5, Sept.-Oct. 1991, pp. 572-584.

8. Priestley, N.; Seible, F.; Xiao, Y.; and Verma, R., "Steel Jacket Retrofitting of RC Bridge Columns for Enhanced Shear Strength. Part 2: Test Results and Comparison with Theory," *ACI Structural Journal*, V. 91, No. 5, Sept.-Oct. 1994, pp. 537-551.

9. Xiao, Y., and Wu, H., "Retrofit of Reinforced Concrete Columns Using Partially Stiffened Steel Jackets," *Journal of Structural Engineering*, ASCE, V. 129, No. 6, 2003, pp. 725-732. doi: 10.1061/(ASCE)0733-9445(2003)129:6(725)

10. Rodriguez, M., and Park, R., "Seismic Load Tests on RC Columns Strengthened by Jacketing," *ACI Structural Journal*, V. 91, No. 2, Mar.-Apr. 1994, pp. 150-159.

11. Lehman, D.; Gookin, S.; Nacamuli, A.; and Moehle, J., "Repair of Earthquake-Damaged Bridge Columns," *ACI Structural Journal*, V. 98, No. 2, Mar.-Apr. 2001, pp. 233-242.

12. Rutledge, S. T.; Kowalsky, M. J.; Seracino, R.; and Nau, J. M., "Repair of Reinforced Concrete Bridge Columns Containing Buckled and Fractured Reinforcement by Plastic Hinge Relocation," *Journal of Bridge Engineering*, ASCE, V. 19, No. 8, 2014, p. A4013001. doi: 10.1061/(ASCE)BE.1943-5592.0000492

13. Haber, Z. B.; Saiidi, M. S.; and Sanders, D. H., "Seismic Performance of Precast Columns with Mechanically Spliced Column-Footing Connections," *ACI Structural Journal*, V. 111, No. 3, May-June 2014, pp. 639-650. doi: 10.14359/51686624

14. Ameli, M. J.; Parks, J. E.; Brown, D. N.; and Pantelides, C. P., "Grouted Splice Sleeve Connection Alternatives for Precast Concrete Bridge Piers in Moderate-to-High Seismic Regions" *Proceedings of the 10th National Conference on Earthquake Engineering*, Anchorage, AK, 2014, 11 pp. doi: 10.4231/D3D50FZ10

15. Ameli, M. J.; Parks, J. E.; Brown, D. N.; and Pantelides, C. P., "Seismic Evaluation of Grouted Splice Sleeve Connections for Reinforced Precast Concrete Column-to-Cap Beam Joints in Accelerated Bridge Construction," *PCI Journal*, V. 60, No. 2, 2015, pp. 80-103.

16. Ameli, M. J.; Parks, J. E.; Brown, D. N.; and Pantelides, C. P., "Seismic Evaluation of Grouted Splice Sleeve Connections for Precast RC Bridge Piers in ABC," *Report* No. UT-14.09, Utah Department of Transportation Research Division, Salt Lake City, UT, 2014, 156 pp.

17. Yan, Z.; Pantelides, C. P.; and Reaveley, L. D., "Fiber-Reinforced Polymer Jacketed and Shape-Modified Compression Members: 1—Experimental Behavior," *ACI Structural Journal*, V. 103, No. 6, Nov.-Dec. 2006, pp. 226-234.

18. AASHTO, "AASHTO Guide Specifications for LRFD Seismic Bridge Design," second edition, American Association of State Highway and Transportation Officials, Washington, DC, 2011, 331 pp.

19. ACI Committee 374, "Guide for Testing Reinforced Concrete Structural Elements under Slowly Applied Simulated Seismic Loads (ACI 374.2R-13)," American Concrete Institute, Farmington Hills, MI, 2013, 18 pp.

20. Hose, Y., and Seible, F., "Performance Evaluation Database for Concrete Bridge Components and Systems under Simulated Seismic Loads," *PEER Report 1999/11*, Pacific Earthquake Engineering Research Center, University of California, Berkeley, Berkeley, CA, 1999, 113 pp., http://peer.berkeley.edu/publications/peer_reports/reports_1999/9911.pdf.

21. Brown, D. N., "Post-Earthquake Repair of Precast Concrete Column-to-Footing Plastic Hinges," MS thesis, University of Utah, Salt Lake City, UT, 2014, 172 pp.

22. Parks, J. E., "Seismic Rehabilitation of Column to Pier Cap ABC Connections and AE Monitoring Assessment," MS thesis, University of Utah, Salt Lake City, UT, 2014, 148 pp.

23. Moran, D., and Pantelides, C., "Elliptical and Circular FRP-Confined Concrete Sections: A Mohr-Coulomb Analytical Model," *International Journal of Solids and Structures*, V. 49, No. 6, 2012, pp. 881-898. doi: 10.1016/j.ijsolstr.2011.12.012

24. ASTM D3039/D3039M-14, "Standard Test Method for Tensile Properties of Polymer Matrix Composite Materials," ASTM International, West Conshohocken, PA, 2014, 13 pp.

25. ACI Committee 440, "Guide for the Design and Construction of Externally Bonded FRP Systems for Strengthening Concrete Structures (ACI 440.2R-08)," American Concrete Institute, Farmington Hills, MI, 2008, 76 pp.